Analysis of Tonal Noise Generating Mechanisms in Low-Speed Axial-Flow Fans

Edward Canepa, Andrea Cattanei, Fabio Mazzocut Zecchin

DIME-Università di Genova via Montallegro 1, I-16145 Genoa, Italy

The present paper reports a comparison of experimental SPL spectral data related to the tonal noise generated by axial-flow fans. A nine blade rotor has been operated at free discharge conditions and in four geometrical configurations in which different kinds of tonal noise generating mechanisms are present: large-scale inlet turbulent structures, tip-gap flow, turbulent wakes, and rotor-stator interaction. The measurements have been taken in a hemi-anechoic chamber at constant rotational speed and, in order to vary the acoustic source strength, during low angular acceleration, linear speed ramps. In order to avoid erroneous quantitative evaluations if the acoustic propagation effects are not considered, the acoustic response functions of the different test configurations have been computed by means of the spectral decomposition method. Then, the properties of the tonal noise generating mechanisms have been studied. To this aim, the constant-Strouhal number SPL, obtained by means of measurements taken during the speed ramps, have been compared with the propagation function. Finally, the analysis of the phase of the acoustic pressure has allowed to distinguish between random and deterministic tonal noise generating mechanisms and to collect information about the presence of important propagation effects.

Keywords: Axial-flow fans, Tonal noise, Acoustic response.

Introduction

Nowadays, low-speed axial-flow fans are employed in several applications, ranging from HVAC systems to automotive cooling units and are requested to fulfil even more stringent requirements in terms of compactness and performances. In most of cases, the geometry of the whole assembly is quite complicated. Compared to the ideal ducted fan, the presence of non-aerodynamically shaped inlet ducts, structural struts and downstream stators may determine a flowfield which is more complex. Such conditions may result in the contemporaneous presence of different noise generating mechanisms. The broadband noise generated at leading and trailing edge typically provides the largest contribution to the overall SPL spectrum, but the low-frequency tonal components are often the major cause of annoyance. Usually, the tonal noise is due to non-uniform inflow conditions. It may be due to large-scale inlet turbulent structures (Homicz and George [1], Majumdar and Peake [2], Hanson [3]), to rotor-stator aerodynamic interaction (Lowson [4], Tyler and Sofrin [5], Kaji and Okazaki [6]), or to the tip-leakage flow (Longhouse [7], Fukano and Jang [8], Kameier and Neise [9]).

The chances to reduce the radiated tonal noise are first related to the identification of the actual source mechanisms. Anyway, this may be difficult since the analysis of the SPL spectrum does not often allow to discriminate between the contributions of different kind of sources. This requires identifying suitable properties, easily obtainable from standard tests.

Furthermore, in many applications, the fan operates at variable speed and, consequently, the peaks may excite the acoustic response function of the assembly at different frequencies, thus superposing with the dependence of the generating mechanism on the rotational speed. The resulting irregular behaviour of tonal components may complicate the analysis and may yield a further cause of annoyance. To overcome such problems, a methodology for discriminating the contribution of propagation effects

in the received noise is used.

In the present work, typical instances of such noise components are analysed and compared by means of methods developed by the authors (Bongiovì and Cattanei [10], Canepa et al. [11], Canepa et al. [12]).

Experimental facility and tested fan

All of the employed experimental data have been acquired during measurement campaigns carried out in the DIME hemi-anechoic chamber, with the fan mounted on a rectangular wooden panel (670 mm × 720 mm, 25 mm thick). The rotor axis has been positioned horizontally and, depending on the case, at heights from the floor between of 1 m and 1.6 m. The microphone has been positioned on-axis between 1 m and 1.18 m upstream, depending on the specific case. The adopted fan, Fig. 1, has $z_R = 9$ evenly spaced blades and is made of polyamide with fiber glass. The rotor is provided with a cylindrical rotating shroud of external diameter $D_{tip} = 460$ mm, the hub has a diameter $D_{hub} = 181$ mm, and the blade chord c varies between 65 mm at the hub and 72 mm at the tip. The rotational speed has been measured by means of the electric motor internal encoder, generating a one-per-revolution TTL signal (in the following the *tacho signal*). The design performance are a flow rate $Q = 1.174$ m^3/s and a static pressure rise $\Delta p = p_{out} - p_0 = 388$ Pa at $\Omega = 3000$ r/min, with air at ambient conditions (20 °C, 101300 Pa). This results in a flow coefficient $\varphi_{des} = Q/(u_{tip}\pi D_{tip}^2/4) = 0.097$ and a pressure coefficient $\psi_{des} = \Delta p/(0.5\rho_0 u_{tip}^2) = 0.121$, where u_{tip} is the blade tip speed. In the present investigation, the fan has been operated at free-discharge conditions, for which $\varphi_{fd} = 0.164$ and $\psi_{fd} = 0$.

Fig. 1 The rotor with the rotating shroud.

The rotor is driven by a PC-controlled brushless servomotor (Danaher AKM42E-ANCNR-00, rated power 1.14 kW at 640 V) supported by a steel structure. This allows a precise positioning by means of a 3-axis system. The structure is fixed to the rectangular wooden panel (670 mm × 720 mm, 25 mm thick). The motor is quieter and more stable than the brushless motors employed in the production units and its noise does not interfere with the aerodynamic one, see Cattanei et al. [13] for the details. The only noticeable effect is a sharp peak at $f \cong 16$ kHz. Such a peak does not influence the noise object of the present study in any relevant way.

The wooden panel has a central circular hole and is supported by a metal frame, thus realizing a free-discharge condition. The standard tip-clearance geometry consists in 5 mm axial and radial gaps and is obtained inserting proper aluminium rings in the hole. The use of different rings allows the tip-gap modification. It is important to underline that, in the adopted measurement configuration, which is quite common for tests on axial fan, the acoustic interference caused by the waves reflected from the chamber floor may impair the free-field condition hypothesis. This effect depends on the distance of the acoustic source from the microphone compared to the distance from the floor and on the source characteristics, i.e. number, location, directivity, and others. Namely, noise due to a coherent, compact source, e.g. a localized wake impinging on the rotor, is strongly affected by such effect, Canepa et al. [11]. Noise due to large-scale inlet turbulent structures, tip-gap flow, and rotor-stator interactionis only slightly affected. The random nature of the broadband noise prevents acoustic interference to take place, hence the power spectral densities of the direct and reflected noise simply sum. Considering the adopted geometry, this leads to an average increase of 0.8 dB in the measured SPL spectrum.

Test configurations

In the present work, four different geometrical test configurations have been adopted, all operated at free discharge condition. Each configuration is aimed at enhancing a single tonal noise generating mechanism, in order to highlight its effect on the whole spectrum.

In the first case (indicated with the acronym of large-scale turbulence, LST) the fan is simply mounted on the rectangular wooden panel with no upstream turbulence control screen adopted, Fig. 3a. In this configuration the main tonal noise generating mechanism is related to the ingested large-scale turbulent structures. It will be shown that in such a case the tip-clearance flow is weak and does not generate an evident tonal component.

The second configuration, Fig. 3b, (indicated with the acronym of rotor-stator interaction, RSI) is similar to the first one, but it is provided with a downstream stator. The employed stator is evenly-spaced and is composed by $z_S = 18$ constant-thickness, cambered vanes of 30 mm chord, Fig. 2. The axial-gap between the rotor blade trailing edge and the stator vane leading edge at the rotor tip is 11 mm. In this last configuration the main active tonal noise generating mechanism is the rotor-stator interaction. The effects related to the tip-clearance flow and the inlet turbulent structures are minor, as it will be

shown in the following. The choice $z_S = 2z_R$ is not realistic since typically z_R and z_S are never integer multiples, but it enhances the SPL at the low BPF harmonics.

Fig. 2 The 18 vanes stator.

The third configuration, Fig. 3c, (indicated with the acronym of tip-gap flow, TGF) consists of a 66 mm long cylindrical duct with a bell-mouth inlet. An upstream screen, consisting in a fabric hood, has been adopted in order to abate the inlet turbulence (turbulence control screen, TCS). In this configuration the presence of the bell-mouth inlet is expected to have an important role in reducing the incoming flow distortions, Maaloum et al. [14]. As a consequence, the main active source of tonal noise is related to the presence of the tip-gap flow. Although the fan is operated at free discharge conditions, the cylindrical duct restrains the tip-gap flow, enhancing the related noise.

In the fourth configuration, Fig. 3d, (indicated with the acronym of turbulent wake, TW) the panel shape has been modified and an extension (outer diameter D_{ext} = 1400 mm) has been added. In order to control the inlet turbulence, as in the TGF case, a hemi-spherical TCS has been employed. To generate a sharp wake, a cylindrical bar of diameter D_{bar} = 12.5 mm has been inserted upstream of the rotor in the upper part of the panel. It extends over the whole blade span and it is located 9.5 mm upstream of the leading edge of the rotor blades. In this configuration the main tonal noise generating mechanism is due to the bar wake impingement on the rotor blade.

Measurement procedure and data processing method

The acoustic pressure data have been acquired and processed by means of a Brüel & Kjær 3560 spectrum analyzer and a pre-polarized ½" free-field microphone.

The measurements have been taken during linear speed ramps (from 500 r/min to 3000 r/min in 1080 s) and at $\Omega = const$. The small angular acceleration, together with the use of the order analysis algorithm, Herlufsen[15], ensured good precision spectral results and allowed to compute the SPL at the harmonics of the rotational frequency, $SPL_n(\Omega)$ (rotational speed based Strouhal numbers $St = 60f/\Omega$, varying from 0 to 80, with resolution $\Delta St = 0.2$). Furthermore, the SPL spectra at constant Ω (range 0 – 20 kHz, 1600 lines with resolution Δf = 12.5 Hz) have been computed. In both kinds of measurements, 100 data records with 50% superposition have been collected. For the constant-Ω spectra, a von Hann window has been employed in order to limit the spectral leakage.

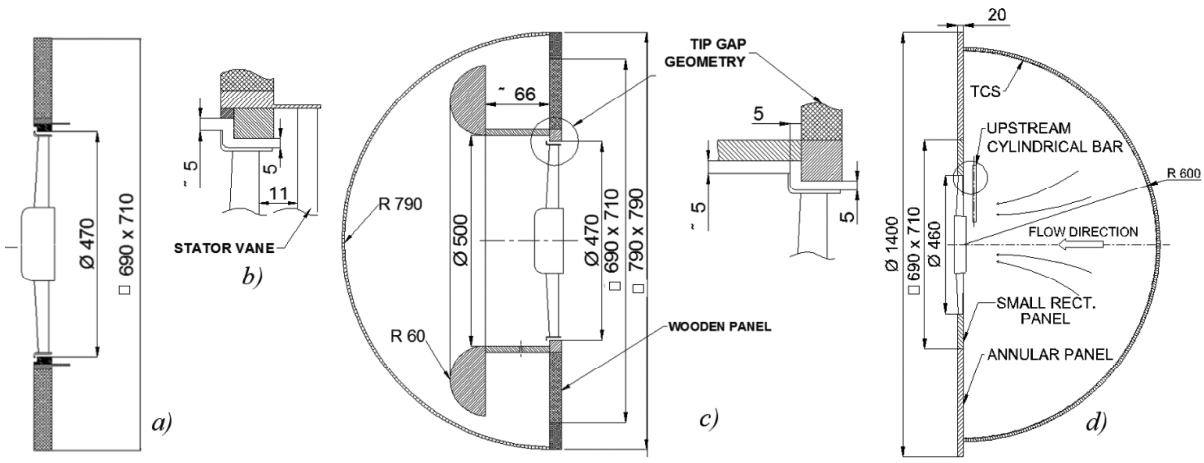

Fig. 3 The four geometrical configurations. a) LST with the standard panel. b) RSIwith details of the tip-gap and the stator. c) TGF with the small TCS and details of the tip-gap region. d) TW with the large TCS and bar.

The SPL spectrum may be defined according to:

$$\mathrm{SPL}(f_k,\Omega)=10\log_{10}\left[\frac{1}{p_{ref}^2}\int_{f_k-\Delta f/2}^{f_k+\Delta f/2}S_{pp}(f,\Omega)df\right] \quad (1)$$

where $S_{pp}(f,\Omega)$ is the one-sided power spectral density of the measured acoustic pressure for a constant-Ω acquisition. Ω has to be considered as a parameter, $f_k = k\Delta f$ and $p_{ref} = 20$ μPa is the reference pressure.

Similarly, SPL_n may be computed as:

$$\mathrm{SPL}_n(\Omega)=10\log_{10}\left[\frac{1}{p_{\mathrm{ref}}^2}\int_{f_n-\Delta f/2}^{f_n+\Delta f/2}S_{pp}(f,\Omega)\mathrm{d}f\right] \quad (2)$$

where $n = St/\Delta St$, $f_n = n\,\Delta St\,\Omega/60$ is the central frequency and $\Delta f = \Delta St\,\Omega/60$ represents the resulting band width. Δf must be small enough in order to allow the broadband noise contribution not to affect the tonal one. Adopting $\Delta St = const$ results in Δf being proportional to Ω. Some parametric tests have shown that the chosen settings yield a sufficient precision of the spectral data, i.e. the random fluctuations usually affecting the plots of spectral quantities are sufficiently limited.

Important information may be obtained from the scaling of constant-ΩSPL spectra based on the similarity theory, Blake [16] or Mongeau et al. [17]: in absence of propagation effects, due to reflections, scattering and diffraction from the fan parts, the SPL spectra relative to different Ω values are expected to collapse on a single curve when the scaled SPL:

$$\mathrm{SPL}_{scaled}(f,\Omega)=\mathrm{SPL}(f,\Omega)-\left(10\log_{10}\Omega^{3+\beta}+K\right) \quad (3)$$

is plotted versus the scaled frequency, i.e. versus the Strouhal number. In Eq. (3) K is an arbitrary constant and the exponent β assumes values about 1 for the trailing edge noise and 3 for the tonal noise.

Differently, when measured during a speed ramp, $\mathrm{SPL}_n(\Omega)$ may experience large variations (of the order of 40 dB), hence preventing from properly studying the SPL_n fluctuations. Therefore, SPL_n may be scaled similarly to the $\mathrm{SPL}(f,\Omega)$, thus allowing the fluctuating part to be extracted, but the linear dependence of Δf on Ω, Eq. (2), requires performing the scaling with a factor of $10\log_{10}\Omega^{4+\alpha}$. If the scaled mechanisms are the same, $\alpha = \beta$ results. Accordingly, the scaled SPL during speed ramps will be considered:

$$D_n=\mathrm{SPL}_n-\left(10\log_{10}\Omega^{4+\alpha}+C_n\right) \quad (4)$$

where C_n is an arbitrary constant.

The phase angle $\varphi_n(\Omega)$ of the Fourier transform of the acoustic pressure (referred to the *tacho signal*) at the BPF and harmonics has been calculated. $\varphi_n(\Omega)$ has a random trend if the noise generating mechanism is not correlated with the rotor position, otherwise it has a linear trend in absence of propagation effects (free-field condition), Canepa et al. [12].

Propagation effects (reflections, scattering and diffraction from surrounding objects and test environments) may result in fluctuations of the acoustic pressure not corresponding to real fluctuations of the source strength. In order to evaluate them, the spectral decomposition method, Bongiovì and Cattanei[10], has been applied. It may be assumed that the received noise depends on frequency through both St and $He = f\,D_{tip}/a_0$, the Helmholtz number based on the speed of sound a_0, resulting in the following structure:

$$\begin{aligned}\mathrm{SPL}(f,\Omega)=&K+10\log_{10}\left(\Omega^{3+\beta}\right)\\&+20\log_{10}F(St)+20\log_{10}G(He)\end{aligned} \quad (5)$$

where $F(St)$ is the non-dimensional source spectral distribution function which depends on the aerodynamic pressure and velocity fluctuations. F is independent of the propagation effects which are included in $G(He)$, the non-dimensional acoustic frequency response function, in the following the propagation function, which depends on the geometry and on the acoustic properties of the whole system (fan and test environment). Under similarity conditions, if Ω varies then the flow velocity varies accordingly, simply resulting in a change in the time scale of the generating mechanism, whereas the time scale of propagation effects remains unchanged. The spectral decomposition method allows to separate the two effects, i.e. to find F and G, comparing the SPL spectra related to several Ω values.

Description of the constant-Ω SPL spectra

The SPL spectra at $\Omega = const$ are the most common representation of acoustic pressure data. Their analysis, Fig. 4 (Ω = 3000 r/min), helps to have an intuitive preliminary understanding of the main phenomena although the detectable information are of limited extent. The features described in the present paragraph are a summary of the analysis reported in Canepa et al. [11, 12, 18]. In the

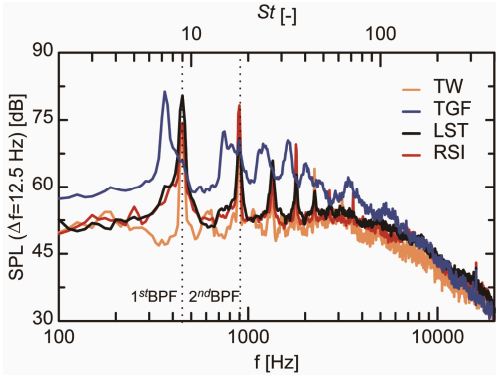

Fig. 4 Constant speed SPL spectra (Ω = 3000 r/min).

LST configuration, at $f < 3$ kHz, the main features are the

tonal noise peaks which clearly emerge from the spectrum up to the 6th BPF harmonic (2.7 kHz). These peaks are due to the presence of large-scale turbulent structures which are stretched by the flow acceleration upstream of the fan, and repeatedly chopped by the rotor blades, Majumdar and Peake [2]. A local, slight increase in the SPL is present at frequencies slightly lower than 1st and 2nd BPF harmonics (dotted vertical lines) and are due to the weak recirculating flow passing through the gap between the rotor shroud and the external aluminium ring.

In the RSI configuration, the SPL spectra appear very similar to the LST one, except for the number and height of detectable peaks. The peaks at the even BPF harmonics are higher than the ones at the odd harmonics, according with the fact that, due to destructive acoustic interference, the rotor-stator interaction may excite only BPF harmonics whose order is a common multiple of z_S and z_R, Lowson [4]. In the present case, $z_S = 2z_R = 18$, thus, only the even BPF harmonics should be presented. The peaks at the odd BPF ones are related to the large-scale turbulent structures, which are presented since no TCS is used in the LST configuration.

For these two configurations, the difference between the SPL at the first BPF is of nearly 4 dB. Actually, no difference should be expected and, likely, the reason for this are acoustic effects which will be deepened in the following. At high frequency, the broadband noise seems to be scarcely influenced by the stator presence, since the spectra are nearly coincident for $f > 3$ kHz.

Compared to the previous configurations, in the TW one, the spectra appear to be modified since the peaks are sharper. This is somehow surprising, since the only geometrical difference is the size of the mounting panel. The broadband part of the spectrum in the whole range of frequency is slightly lower than in the LST and RSI configurations. This feature is consistent with the presence of the TCS which abates both large- and small-scale inlet turbulence, thus reducing also the leading edge noise which is due to the latter. A bump, of about 7 dB, is present in the range 500 Hz $< f <$ 700 Hz, which is probably due to the von Karman vortex release from the bar. Compared to the previous configurations, in the TW one, the overall behaviour of the spectrum is less regular.

In the TGF configuration, the presence of the cylindrical duct modifies both the incoming flow and the tip-gap flow patterns. Namely, the strong modification occurring in the blade tip region results in a strong increase of the whole SPL spectrum below 4 kHz. Compared to the other three cases, a growth of nearly 10 dB takes place. The peaks at the BPF harmonics are largely reduced due to the presence of the TCS, while new local maxima appear at frequencies slightly lower than the BPF harmonics: characteristic values are, approximately, St = 7.2, 15, 23.2, 32.4, and 41.2 (between 0.82 and 0.89 times BPF). These new peaks are due to the recirculating flow hailing from the tip-gap and the associated flow structures impinge on the rotor at frequencies lower than BPF and harmonics, due to the positive pre-rotation, Longhouse [7], Fukano and Jang [8], Kameier and Neise [9]. For $f > 4$ kHz, the peaks disappear and the typical asymptotic trend is recovered. The increase in the broadband part is probably due to the small-scale turbulence contained in the recirculating flow which increases the leading-edge noise. In the high frequency part of the spectrum, the broadband noise is only a few dB different from the LST and RSI configurations, and also the asymptotic trends are only slightly different.

The information which can be inferred from the analysis of the SPL spectra are important and may allow to evaluate the acoustical behaviour of a fan. Unfortunately, in many applications, the fan operates at variable speed and transferring the results obtained from data collected at a certain Ω to other rotational regimes is not straightforward. Furthermore, differences between the geometry of different test environments or the actual one may result in differences in the spectra.

Scaling of the constant-Ω SPL spectra

In order to evaluate the possibility of scaling the spectra, the SPL, obtained from measurements taken at Ω = 2400, 2700 and 3000 r/min have been scaled according to Eq. (3), Fig. 5. $\beta = 1$ has been employed. In order to allow the comparison of scaled spectra, SPL_{scaled} have been plotted versus St.

In both the LST and RSI cases, with the exception of some peak and limited parts, the three curves related to the different Ω collapse in a band of about 3 dB width. In the TGF case, the dispersion is slightly larger, but many parts show a worse collapse.

In the TW configuration, the broadband parts are spread within a broader range (up to 6 dB) and the peaks show a very important dispersion, which may even reach 15 dB at the first BPF harmonic.

The above discussion shows that the scaling procedure, though simple and useful, may easily become misleading. The reasons for this may be two: first, the use of a unique scaling exponent for the whole spectrum may not be correct since different noise generating mechanisms may scale differently; second, the presence of strong propagation effects may substantially modify the received noise, thus impairing the possibility of performing a velocity scaling.

Description of the SPL during the speed ramps

A better insight into the problem may be gained by means of D_n, Eq. (4), evaluated at the relevant St values. D_n may be represented in a contour plot as a function of

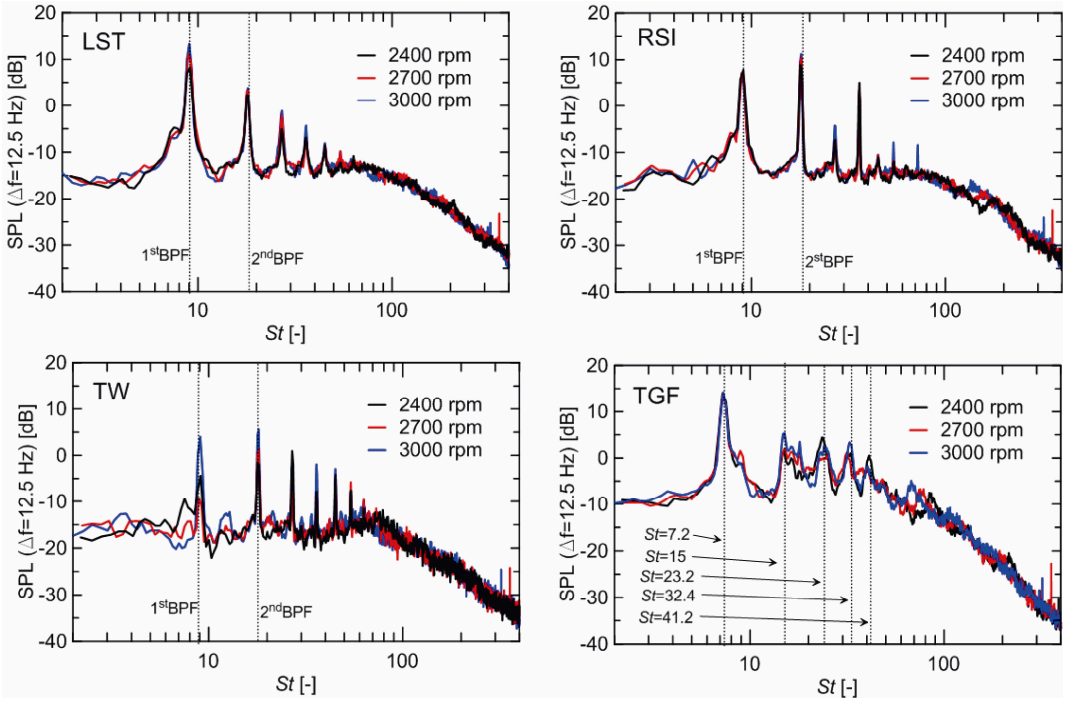

Fig. 5 The SPL_{scaled} for the four configurations (Ω = 2400, 2700, 3000 rpm).

St and Ω, Fig. 6. A noise generating mechanism is generally characterized by a fixed *St*, while propagation effects take place at fixed frequency. Then, in such a plot, a $f = const$ line is a hyperbola of equation $St = 60f/\Omega$, but it becomes a straight line $\log(St) = \log(60\,f) - \log\Omega = const - \log\Omega$ when plotted in a bi-logarithmic plot. Thus, propagation phenomena are identified as inclined strips, while noise generating mechanisms are vertical ones.

In the LST configuration, a D_n valley at f = 180 Hz indicates that propagation effects are probably present, possibly due to the test environment. Similarly, in the RSI case, a valley may be noticed at f = 270 Hz. In the TW configuration an analogous feature is present at f = 400 Hz. Different from the previous cases, this valley is very deep: a strong reduction (more than 10 dB) at the first BPF harmonic takes place in the range $2400 < \Omega < 2700$ r/min. In the TGF configuration, a valley at f = 500 Hz and a crest at 900 Hz are present. The first reduces $D_{n,}$ of nearly 5 dB, while the second one increases it of approximately 7 dB. The analysis of the D_n distributions for all the considered configurations suggests some interesting considerations about the scaling process. Fixing Ω means cutting one of the previous contour plots along an horizontal line. If propagations effects are present, the $\Omega = const$ line will cut across the inclined strips and, in the crossing region, both the measured SPL and the scaled one will be affected by uncertainties which may impair the correct evaluation of the noise generation mechanism dependence on Ω. Some examples may be found in Fig. 5 for the RSI and TGF cases. Particularly in the first one, for Ω = 2400 r/min at St = 180 a small bump is present in the SPL_{scaled} spectrum. As the rotational speed is increased the bump moves towards lower values of *St* (St = 150 for Ω = 2700 r/min and St = 120 for Ω = 3000 r/min). In the TGF case, a similar behaviour may be found in the range $60 < St < 90$.

This kind of contour plots results in an immediate and reliable way to perform a qualitative analysis. Differently, if a quantitative one is required, representing D_n by means of curves may be more appropriate.

As an example, in Fig. 7 the curves representing the scaled SPL at the first six BPF harmonics for the LST, RSI and TW configurations are depicted. In the TGF case, the curves are related to the five previously identified tonal peaks at approximately St = 7.2, 15, 23.2, 32.4, and 41.2 (indicated as $D_I - D_V$ respectively). The D_n curves are represented as a function of $f = St\Omega / 60$. Moreover for each configuration the propagation function $G(f)$ is also reported. The D_n curves are typically affected by random errors of some dB, which introduce undesired point to point fluctuations which render the trend less clear. Hence, a 5 points running average has been employed to smooth them. It is also useful to remind that in the adopted spectral decomposition method, Bongiovì and Cattanei [10], most of the employed spectral data are related to the broadband noise. Consequently, the evaluated propagation function is foremost dependent on the broadband part of the SPL spectrum and typically shows

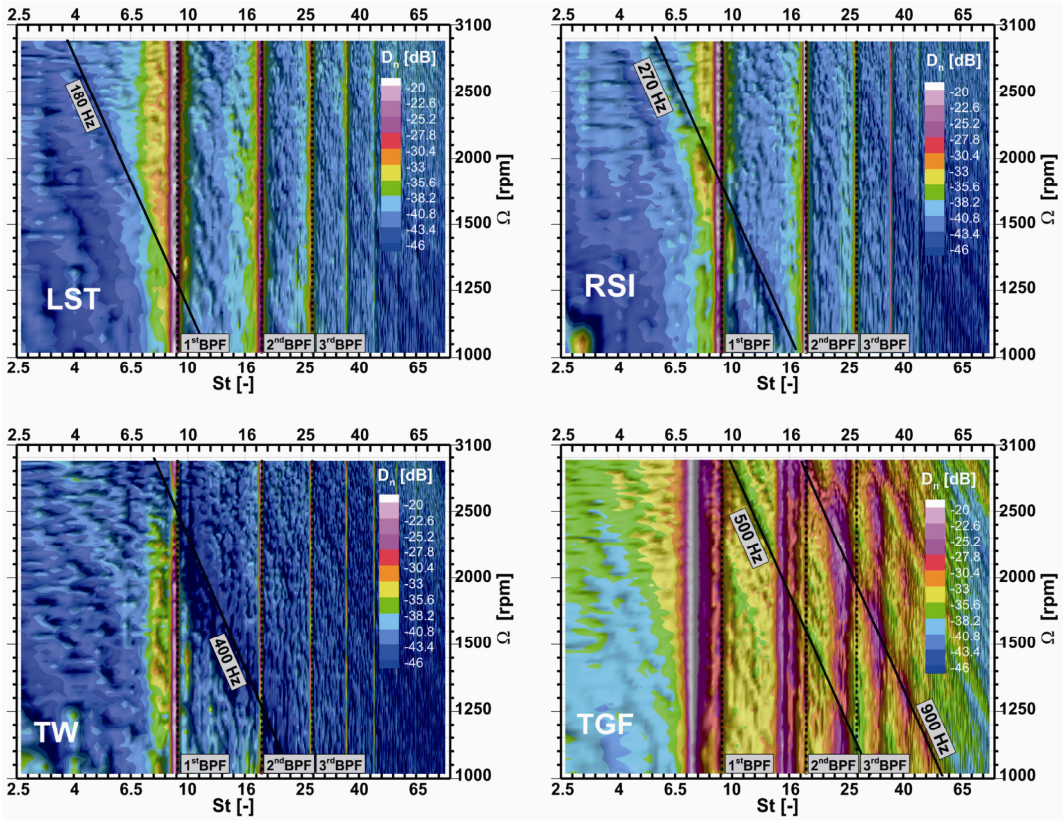

Fig. 6 Contour plot of D_n for all the four configurations.

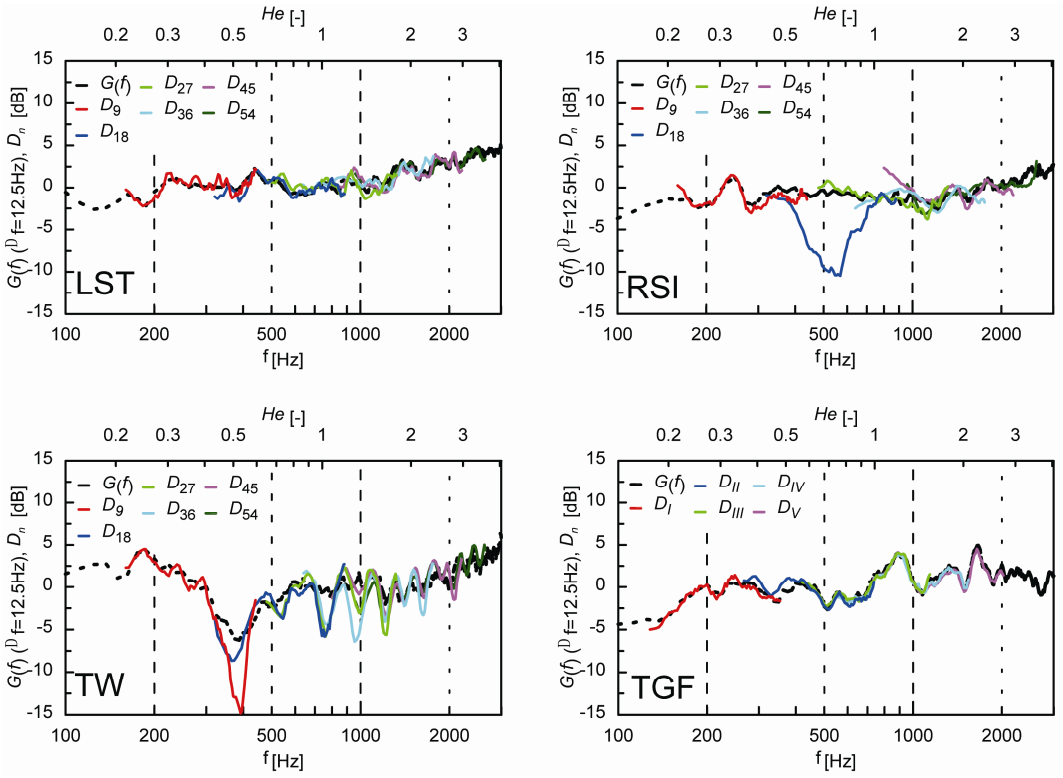

Fig. 7 Distributions of the D_n and the propagation function $G(f)$ for all the four configurations.

a smooth trend when plotted vs. f.

Generally speaking, $G(f)$ is related to the Green's function evaluated at the point where the source is located, Mongeau et al. [17]. Thus, G may depend on the source position on the blade, and hence different noise generation mechanisms may be related to different $G(f)$. Particularly, in case of noise sources which are distributed on the whole blade surface, some kind of spatial average of the Green's function may be expected. As a consequence, the tonal noise may be affected by a propagation function different from the one related to the broadband noise.

Considering that, during the speed ramp, a tonal component sweeps the acoustic transfer function of the system, Canepa et al. [11] and Margetts [19], then D_n may be regarded as a piece of the propagation function associated to a constant-St generation mechanism. Since the D_n curves are defined up to a constant and an exponent, see Eq. 4, a trial and error procedure is needed to try to let the D_n curves collapse on each other and on $G(f)$. If a unique propagation function is present, then a unique trend may be found between the D_n curves and $G(f)$.

In the LST configuration, the D_n curves may be clearly superposed to $G(f)$. This behaviour indicates that for this configuration the active tonal noise generation mechanism and the broadband one are influenced by the same propagation function. Indeed, large-scale turbulent structures impinge on all blades at random positions, thus, the resulting tonal noise generating mechanism is probably characterized by a behaviour, in terms of spatial distribution, sufficiently similar to the broadband noise which is generated continuously along the whole blade span by all blades.

In the RSI configuration, the D_n curves related to the odd BPF harmonics (D_9, D_{27}, D_{45}) may be properly superposed to the broadband $G(f)$, while the D_{18} trend is characterized by a deep minimum at $f = 550$ Hz (nearly 10 dB lower than $G(f)$). A possible explanation of this behavior may be that, in this configuration, the odd BPF harmonic tonal noise is generated by the same generation mechanism as in LST, i.e. the large-scale turbulent structures. Differently, the noise due to the rotor-stator interaction is probably generated by sources which are well localized on both the rotor blades and stator vanes, hence resulting in a different propagation function from the broadband mechanism.

In the TW configuration a wavy behaviour is presented for both $G(f)$ and the D_n curves. A dip at 400 Hz is clearly visible, and in the range 600 Hz $< f <$ 2000 Hz a regularly oscillating trend may be observed with a separation between the maxima/minima of nearly 200 Hz and a peak to valley variation of more than 5 dB. Generally speaking, this behaviour is very interesting, and is probably due to the combined presence of two different acoustic effects, Canepa et al. [11]: the dip is ascribed to the large circular wooden panel, while the oscillating trend is due to the floor presence. Hence, this geometrical configuration results in strong propagation effects which may largely impair the correct evaluation of the sources strength. As a consequence, the test environment has to be carefully studied in order to avoid such effects.

In the TGF case, the D_n curves may be fairly superposed to the $G(f)$ one, as in the LST one, thus indicating that the tip-gap flow generating mechanism has a behaviour which is quite similar to the ingestion of large-scale turbulent structures, at least in terms of source spatial distribution.

For the sake of completeness, the comparison between the different propagation functions is reported in Fig. 8. Comparing the values of the LST and RSI curves at $f = 450$ Hz it is possible to observe that the former is nearly 5 dB larger than the latter. This aspect allow explaining the difference seen in the SPL spectrum (Fig. 4) for the first BPF harmonic peak. Another interesting aspect may be highlighted considering the oscillations of nearly 5 dB amplitude in the TGF curve at $f > 600$ Hz. This is a propagation effect probably due to the cylindrical duct. Moreover, such oscillations may explain the non-complete collapse of the SPL related to the tip-gap peaks.

The plots of φ_{18} (Ω) during a speed ramp are reported in Fig. 9 in which, for brevity, only the LST and RSI configurations have been considered. In order to clarify the φ_{18} characteristics, also the D_{18} curve for the RSI case has been added. According to the random nature of the LST noise, a random trend of φ_{18} may be detected. Differently, in the RSI case, the D_{18} generation mechanism should have a deterministic nature, being related to the mutual circumferential position of the rotor and the stator. Therefore a linear trend of φ_{18} is expected. As a matter of fact, its behaviour appears different from the expected one: two linear parts are presented with a sudden decrease of about 150 deg between 450 and 550 Hz (i.e. between 1500 and 2000 r/min). Two reference lines characterized by a – 1.06 deg/Hz slope have been added, since they represent the phase trend typical of free-field propagations for the present configuration, see Canepa et al. [12]. Two bumps are presented at 200 and 300 Hz and are nearly coincident with oscillations in the D_{18} trend. In the region 450 Hz $< f <$ 550 Hz, a strong phase shift may be identified. In the same frequency range, D_{18} is characterized by the large dip already identified in Fig. 7, which has been related with the presence of propagation effects. Hence, it may be inferred that the analysis of the φ_n plots provides complementary information about both the prevailing generation mechanism and the presence of acoustic effects due to the test environment and the fan assembly.

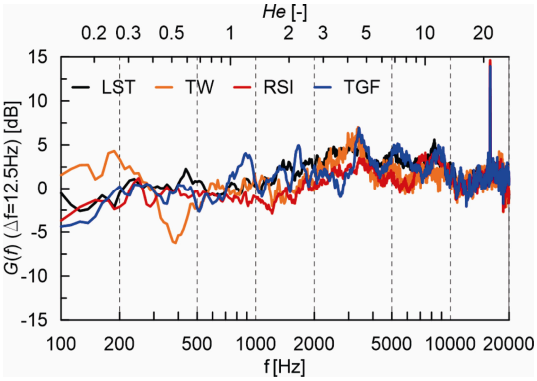

Fig. 8 Propagation functions $G(f)$.

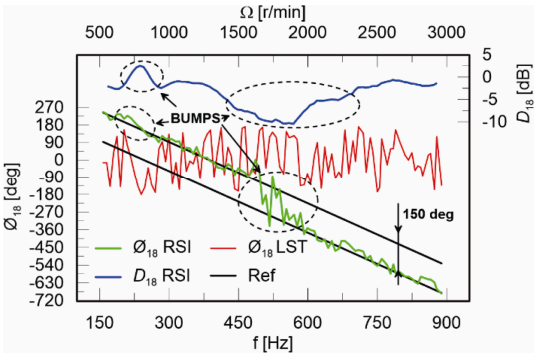

Fig. 9 Phase angle ϕ_n and D_n at the 2nd BPF harmonic

Conclusions

Experimental spectral data concerning the tonal noise generated by an axial-flow fan rotor operating in different configurations have been compared, with the aim of providing possible ways of discriminating between different tonal noise generating mechanisms. A set of easily obtainable acoustic quantities, namely constant-Strouhal number SPL and phase, have been presented, which also allow identifying the propagation effects due to the test environment. The fan has been operated at free-discharge condition and has been employed in four different geometrical configurations designed to activate four different tonal noise generating mechanisms: large-scale turbulent structures, tip-gap flow, turbulent wakes, and rotor-stator interaction. Moreover, the four configurations also introduce different acoustic propagation effects which affect the SPL spectra in a different way. The measurements have been taken in a hemi-anechoic chamber during low-acceleration rotational speed ramps and at constant rotational speed.

The analysis of the usual SPL spectra collected at constant rotational speed allows to identify some basic features of the different generating mechanisms. Unfortunately, in many applications, the fan operates at variable speed, and caution has to be used in extending the results obtained from data collected at a certain rotational speed to other rotational regimes. Furthermore, the acoustic properties of operating environment may be different from the testing one.

The analysis of the constant-speed scaled SPL indicates that the scaling procedure may lead to erroneous conclusions, especially when a quantitative analysis is required, since propagation effects cannot be eliminated. Conversely, the acquisition of the acoustic pressure during a speed ramp allows to compute the SPL at fixed Strouhal number, which is usually related to a single noise generating mechanism. The latter, once scaled, provides quantitative information about the tonal noise generating mechanisms and evidences how the presence of propagation effects may impair the correct evaluation of the dependence of the noise source on the rotational speed. Finally, the phase angle of the acoustic pressure FFT provides further information about both the random or deterministic nature of the prevailing generating mechanism and the presence of propagation effects.

Acknowledgements

The authors kindly acknowledge Johnson Electric Asti srl for having provided the tested fan and Università di Genova for the financial support to the present work.

References

[1] Homicz, G.F., George, A.R., Broadband and discrete frequency radiation from subsonic rotors, *Journal of Sound and Vibration*, 1974, Vol. 36(2), pp. 151–177.

[2] Majumdar, S.J., Peake, N. Noise generation by the interaction between ingested turbulence and a rotating fan, *Journal of Fluid Mechanics*, 1998, Vol. 359, pp. 181–216.

[3] Hanson, D.B., Spectrum of rotor noise caused by atmospheric turbulence, *Journal of Acoustical Society of America*, 1974, 56(1), pp. 110–26.

[4] Lowson, M.V., Theoretical analysis of compressor noise, *Journal of Acoustical Society of America*,1970, 47(1), pp. 371–385 (Part 2).

[5] Tyler, J., Sofrin, T., Axial flow compressor noise studies, SAE Transactions, 1962, 70: 309–332.

[6] Kaji, S, Okazaki, T., Generation of sound by rotor-stator interaction, *Journal of Sound and Vibration*, 1970, Vol. 13(3), pp. 281–307.

[7] Longhouse, R., Control of tip-vortex noise of axial flow fans by rotating shrouds, *Journal of Sound and Vibration*, 1978, Vol. 58(2), pp. 201–214.

[8] Fukano, T., Jang, C.-M., Tip Clearance Noise of Axial Flow Fans Operating at Design and Off-Design Condition, *Journal of Sound and Vibration*, 2004, Vol. 275, pp.

1027–1050.

[9] Kameier, F., and Neise, W., Experimental Study of Tip Clearance Losses and Noise in Axial Turbomachines and Their Reduction, *ASME Journal of Turbomachinery*, 1997, Vol. 119, pp. 460–471.

[10] Bongiovì, A., Cattanei, A., Spectral decomposition of the aerodynamic noise generated by rotating sources, *Journal of Sound and Vibration*, 2011, Vol. 330, pp. 136–152.

[11] Canepa E, Cattanei A, Mazzocut Zecchin F. Installation effects on the tonal noise generated by axial flow fans, *Journal of Sound and Vibration*, 2015, Vol. 340, pp. 167–189.

[12] Canepa, E., Cattanei, A., Mazzocut Zecchin, F., Effect of the rotor–stator gap variation on the tonal noise generated by axial-flow fans, *Applied Acoustics*, 2015, Vol. 94, pp. 29–38.

[13] Cattanei, A., Milanese, G., Parodi, D., An Experimental Study of the Effect of the Test Configuration on the Noise Generated by Axial Flow Fans, AIAA Paper 2009–3289, 30th AIAA Aeroacoustics Conference, 2009.

[14] Maaloum, A., Kouidri, S., Bakir, F., Rey, R., Effect of inlet duct contour and lack thereof on the noise generated of an axial flow fan, *Applied Acoustics*, 2003, Vol. 64, pp. 999–1010.

[15] Herlufsen, H., Order Analysis Using Zoom FFT, Brüel & Kjaer Application Notes, No. 012-81, 1981, URL: http://www.bksv.com/doc/012-81.pdf.

[16] Blake,W.K., Mechanics of flow-induced sound and vibration, Academic Press, Orlando, 1986.

[17] Mongeau, L., Thompson, D.E., McLaughlin, D.K., Sound generation by rotating stall in centrifugal turbomachines, *Journal of Sound and Vibration*, Vol. 163, No. 1, 1993, pp. 1–30.

[18] Canepa, E., Cattanei, A., Mazzocut Zecchin, F., Milanese, G., Parodi, D., Experimental study and velocity scaling of the tip-leakage noise generated by low-speed axial-flow fans, AIAA-paper 2014–3347, 35th AIAA aeroacoustics Conference, 2014.

[19] Margetts, E.J., A demonstration that an axial fan in a ducted inlet ducted outlet configuration generates predominantly dipole noise, *Journal of Sound and Vibration*, 1987, Vol. 117, pp. 399–406.